

# Boosting 5G mm-Wave IAB Reliability with Reconfigurable Intelligent Surfaces

Paolo Fiore\*, Eugenio Moro\*, Ilario Filippini\*, Antonio Capone\*, and Danilo De Donno†

\*ANTLab - Advanced Network Technologies Laboratory, Politecnico di Milano, Milan, Italy

†Milan Research Center, Huawei Technologies Italia S.r.l, Milan, Italy

Email: {paolo.fiore, eugenio.moro, antonio.capone, ilario.filippini}@polimi.it, danilo.dedonno@huawei.com

**Abstract**—The introduction of the mm-Wave spectrum into 5G NR promises to bring about unprecedented data throughput to future mobile wireless networks, but comes with several challenges. Network densification has been proposed as a viable solution to increase RAN resilience and newly introduced IAB is considered as a key enabling technology with compelling cost-reducing opportunities for such dense deployments. Reconfigurable Intelligent Surfaces (RISes) have recently gained extreme popularity as they can create Smart Radio Environments by EM wave manipulation. Recent studies have shown how this technology can behave as inexpensive passive relays. However, it is not yet clear what role this technology can play in a large RAN deployment. With the scope of filling this gap, we propose a new mm-Wave IAB planning tool where RISes can be installed alongside base stations to maximize the network resilience against blockages due to nomadic obstacles and human self-blocking. Numerical results show how adding RISes to IAB deployments can provide high levels of blockage resistance, while they also significantly reduce the overall network planning cost.

## I. INTRODUCTION

Recently, considerable efforts have been put into the standardization of millimetre-wave (mm-Wave) communications into 5G NR. This newly available spectrum enables high mobile throughput while solving the spectrum scarcity at sub-6 GHz bands [1]. However, such high frequencies bring in a series of challenges when designing Radio Access Networks (RAN), mainly due to the adverse propagation of mm-Waves.

Numerous solutions have been proposed to address these specific challenges. In particular, sophisticated antenna arrays have been developed to overcome extreme path losses. However, the issue of blockages due to opaque obstacles interrupting the line of sight needs to be addressed at a network level. Indeed, dense Base Station (BS) deployment can provide the reliability level needed by 5G requirements, as failed radio links can be easily recovered by connecting to alternative BSs [2]. Recently proposed Integrated Access and Backhaul (IAB) promises to cut down on the cost and complexity deriving from such dense networks, and thus, it is among the most promising enablers for mm-Wave RAN [3].

As per 3GPP specifications, an IAB RAN generally consists of a network of base stations (IAB-nodes), among which one (IAB-donor) has direct, wired access to the core network, while the rest are interconnected through in-band wireless backhauling. Consequently, IAB brings about affordable dense networks without the need to densify backhaul wiring. Moreover, IAB is particularly effective when applied to mm-

Wave RAN: thanks to the vast wireless capacity and highly directional transmissions, it is possible to obtain dense access networks by installing only a few pricey donors.

Reconfigurable Intelligent Surfaces (RISes) are gaining momentum as the latest thing in advanced EM technologies [4]. They have proven to be effective in focusing impinging radio waves towards arbitrary directions, effectively behaving as passive relays [5]. Their expected low production and operation costs have the potential of increasing the cost-effectiveness of dense mm-Wave networks. However, while it has been shown that RISes have relaying capabilities in small and controlled scenarios [6], it is not yet clear what role this technology can play in a large RAN deployment.

This work aims to fill this gap in the literature by proposing a new mm-Wave IAB RAN planning tool where RISes can be installed alongside IAB nodes and donors. The objective of the planning is to maximize blockage resilience while guaranteeing an adequate coverage level to each user of the network. In our experimental campaign, we compare the RIS-enabled planning against a baseline traditional IAB network. After a network planning phase, opaque obstacles are randomly dropped in the service area, allowing an evaluation of the blockage resilience during normal network operation. Results show that while RISes cannot substitute IAB nodes completely, the two technologies work well together to maintain high levels of network resilience, with deployment costs lower than those of IAB-only planning.

The rest of the paper is organized as follows. In Section II, we discuss related works on the planning of IAB networks and RISes. In Section III, we introduce the proposed planning approach and describe the related MILP model. The results of the experimental campaign are showcased in Section IV, while Section V concludes the paper with some final remarks.

## II. RELATED WORKS

Despite the abundant literature on wireless multi-hop network planning started more than a decade ago [7], [8], mm-Wave IAB RANs have sparked a new interest in planning methodologies soon after the first architectural specifications, due to the peculiar aspects of mm-Wave communications. Stochastic models [9], greedy algorithms [10], and GA-based techniques [11] have been very recently proposed to design these networks. However, a complete optimization model for these networks considering capacity and reliability issues in the presence of obstacle blockages is still missing.

RISes are a very recent technological outcome [12], [13]. Nevertheless, they are the main topic of an increasing number of recently published papers. They have emerged as a more energy-efficient and less costly alternative to traditional decode-and-forward approaches [14]–[16]. Therefore, the main research direction to date has aimed to evaluate their link-level performances to establish the best RIS configuration.

Only two works consider the impact of RISes at a network level, particularly addressing the fundamental problem of obstacle blockages. Authors in [17] propose an analysis based on stochastic geometry to study the relationship between the density of RISes, network devices, obstacles and network availability. Some of the authors of this article propose in [18] a first optimization model to plan mm-Wave 5G RANs considering the RIS placement. This article extends the work by considering a different network architecture based on the IAB paradigm, the effect of obstacle blockages, and a new planning approach that leverages multi-connectivity and guarantees spatial diversity among access links.

To the best of our knowledge, this is the first work proposing a complete optimization model *jointly* 1) addressing the network planning of mm-Wave IAB radio access networks, 2) including the RIS placement and 3) improving the network reliability in response to sudden obstacles.

### III. RIS-ENHANCED COVERAGE MODEL

This section describes a coverage planning formulation where the blockage-resilience of a mm-Wave IAB access network is boosted by reconfigurable intelligent surfaces (RISes). We consider RISes as *passive beamformers*, capable of focusing an impinging radio wave towards arbitrary directions. This capability can be exploited at a network level to create a reflected radio path between a transmitter and a receiver, as RISes effectively behave as passive relays. The tuple comprising a transmitter, a receiver and an RIS assisting the communications is known as Smart Radio Connection (SRC) [18] and extends the well-known concept of Smart Radio Environment [19].

SRCs can thus naturally provide dual-connectivity, namely connecting the UE through multiple radio links, which is effective in reducing outages due to obstacle obstructions in mm-Wave access networks [2]. Indeed, an RIS can be installed and configured such that it creates an alternative reflected radio path, which can be exploited to ensure continuity of service in case of direct link obstructions<sup>1</sup>, thus enhancing the mm-Wave network reliability against blockages.

However, a single but sizeable nomadic obstacle could interrupt both the primary and reflected path if these present low angular separation, leading to an SRC outage and decreasing the solution's efficacy. An example is provided in Figure 1a, where poorly angular-separated BS-UE and RIS-UE links are blocked by a single obstacle. On the other hand, the spatial

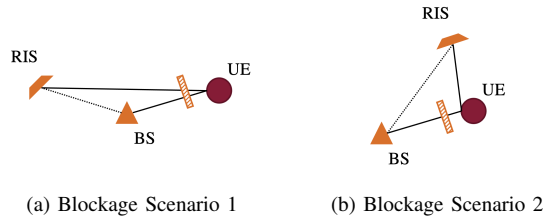


Fig. 1: SRC blockage scenarios for different angular separation values.

configuration in Figure 1b shows how a more significant angular separation can protect the SRC against obstructions of the same size. Moreover, a large angular separation between primary and reflected links can mitigate the well-known effect of *self-blockage*, caused by the human body of the device holder interrupting the line of sight [20].

Link length represents another factor influencing the network resilience that can be controlled during the network planning phase. Indeed, longer radio connections naturally experience higher probabilities of being blocked by one or more obstacles [21].

It is clear now that, independently of the link recovery procedure employed during network operation, a reliable mm-Wave RAN design coincides with a careful installation of BS and RIS during the planning phase. For this reason, our coverage planning formulation takes into account both link lengths and angular separation to maximize the network resilience against nomadic obstacles and self-blockage events.

Similarly to what has been done in other coverage planning works [2], [7], we consider a set  $\mathcal{C}$  of Candidate Sites (CSs) over a geographic area covered by a mm-Wave access service. Each candidate site represents the position where a donor, an IAB node or an RIS can be installed. A set of Test Points (TPs)  $\mathcal{T}$  represents the UE distribution over the same area.

Physical parameters and propagation characteristics, such as transmit power, receiver sensitivity and attenuation losses, are captured by a binary activation link parameter  $\Lambda_{t,c,r}^{\text{SRC}}$ . This is equal to 1 only when an SRC can be established between TP  $t \in \mathcal{T}$ , a donor or an IAB node installed in CS  $c \in \mathcal{C}$  and a RIS in CS  $r \in \mathcal{C}$ . Moreover, fixed obstacles across the geographic area interrupting any line of sight can be modelled by setting the corresponding link activation parameter to 0. Similarly, binary parameter  $\Lambda_{c,d}^{\text{BH}}$  indicates whether two BSs in CSs  $c, d \in \mathcal{C}$  can establish a radio backhaul link.

TP and CS are fixed, and thus achievable downlink rates in backhaul and access can be computed according to radio device characteristics and channel models. The extreme directivity of mm-Wave downlink transmissions limits the interference effects, and we assume these achievable rates to be unaffected by simultaneous transmissions [2]. For each SRC  $\langle t, c, r \rangle$ , parameter  $V_{t,c,r}^{\text{DIR}}$  denotes the achievable TP  $t$  downlink rate obtained through the direct link with the BS  $c$ . On the other hand,  $V_{t,c,r}^{\text{REF}}$  indicates the achievable rate when the RIS-reflected radio path is employed. Finally, the capacity of a backhaul link established between two BSs  $c$  and  $d$  is

<sup>1</sup>Note that, since IAB donors/nodes and RISes are installed higher than UEs, backhaul and BS-RIS links are intrinsically more stable. Therefore, we do not consider blockages for them, apart from those given by fixed obstacles populating the geographic area.

denoted by the parameter  $U_{c,d}$ .

We consider each TP as covered when the planning is such that a specific traffic demand can be guaranteed on both the direct and reflected link. In particular, the parameter  $D$  represents the demand to be guaranteed by the line of sight connection with the BS. On the reflected link, a fraction  $\xi$  of the traffic demand  $D$  is guaranteed. This represents the throughput available to a TP through the backup link, which can be activated when the primary link is experiencing outages.

We assume continuous monitoring of the direct link during regular network operation. Whenever an obstruction is detected, the RIS of the SRC can be reconfigured to offer the alternative reflected path. In this case, the TP would experience a throughput degradation given by parameter  $\xi$ , but the connectivity would be preserved.

As previously mentioned, our model favours the activation of those SRCs offering high angular separation between the direct and reflected lines of sight. This is achieved by considering parameter  $\Theta_{t,c,d}$ , that denotes the smallest angle between CSs  $c$  and  $d$ , as seen from TP  $t$ . Parameter  $L_{t,c}$ , representing the distance between TP  $t$  and CS  $c$ , is used to control the access link length.

Instantaneous reconfiguration of RIS reflecting elements is assumed, such that the surface can switch to assist different SRCs. However, we allow up to 1 TX-RX pair to be RIS-assisted at any time, leading to RIS being shared among SRCs on a time basis. These previous assumptions may result to be technologically challenging for current RIS hardware manufacturers. However, we believe them to represent a realistic technological maturity level which should be considered for a robust investigation of potential RIS benefits. RIS prototypes have shown to present a limited array field of view [9], similarly to what happens for uniform planar antenna arrays. Consequently, the orientation of each installed RIS needs to be such that the lines of sight of the base stations/test points of all SRCs which the RIS is assigned to all fall inside the RIS's field of view. In this work, we define a horizontal field of view angle  $F$ , and we discard the vertical field of view<sup>2</sup>.

Finally, the entire network plan is limited to a budget value  $B$ . Prices  $P^{\text{IAB}}$ ,  $P^{\text{RIS}}$  represent the costs of installing an IAB and a RIS in any CS, respectively<sup>3</sup>.

Here follow the decision variables on which the proposed planning model is based:

- $y_c^{\text{DON}}, y_c^{\text{IAB}}, y_c^{\text{RIS}} \in \{0, 1\}$ : installation variables equal to 1 if a donor, an IAB node or a RIS is installed in CS  $c \in \mathcal{C}$ , 0 otherwise,
- $x_{t,c,r} \in \{0, 1\}$ : SRC activation variable, equal to 1 if RIS in  $r \in \mathcal{C}$  assists the communication between BS in  $c \in \mathcal{C}$  and TP  $t \in \mathcal{T}$ , 0 otherwise,
- $z_{c,d} \in \{0, 1\}$ : backhaul link activation equal to 1 if BS in  $c \in \mathcal{C}$  is connected to BS  $d \in \mathcal{C}$ , 0 otherwise,

- $f_{c,d} \in \mathbb{R}^+$ : backhaul traffic flowing from BS  $c \in \mathcal{C}$  to BS  $d \in \mathcal{C}$ ,
- $w_c \in \mathbb{R}^+$ : traffic flowing from the core network into donor  $c \in \mathcal{C}$  through a wired connection,
- $t_c^{\text{TX}}, t_c^{\text{RX}} \in [0, 1]$ : for any BS  $c \in \mathcal{C}$ , the fraction of time spend in transmission and reception, respectively,
- $\delta_r \in [0, 2\pi]$ : RIS orientation variable, azimuth with respect to a reference direction,
- $\tau_{t,c,r} \in [0, 1]$ : fraction of time spent by RIS  $r \in \mathcal{C}$  while being configured to create a secondary radio path between BS  $c \in \mathcal{C}$  and TP  $t \in \mathcal{T}$ ,
- $\lambda_t \in \mathbb{R}^+$ : average between direct (with BS) and secondary access (with RIS) link lengths covering TP  $t \in \mathcal{T}$ ,
- $\theta_t \in [0, \pi]$  angular separation between direct and secondary links covering TP  $t \in \mathcal{T}$ .

With the given notation, parameters and decision variables, we now introduce a MILP (Mixed Linear Linear Programming) formulation of the IAB network coverage planning problem with RISes:

$$\max \sum_{t \in \mathcal{T}} \left\{ \mu \sum_{t \in \mathcal{T}} \frac{\theta_t}{\Theta} + (1 - \mu) \sum_{t \in \mathcal{T}} \frac{t_t}{\bar{L}} \right\} \quad (1a)$$

s.t.:

$$y_c^{\text{IAB}} + y_c^{\text{RIS}} \leq 1 \quad \forall c \in \mathcal{C} \quad (1b)$$

$$y_c^{\text{DON}} \leq y_c^{\text{IAB}} \quad \forall c \in \mathcal{C} \quad (1c)$$

$$\sum_{c \in \mathcal{C}} y_c^{\text{DON}} = 1 \quad (1d)$$

$$\sum_{c \in \mathcal{C}} (P^{\text{IAB}} y_c^{\text{IAB}} + P^{\text{RIS}} y_c^{\text{RIS}}) \leq B \quad (1e)$$

$$x_{t,c,r} \leq \Lambda_{t,c,r}^{\text{SRC}} (y_c^{\text{IAB}} \wedge y_r^{\text{RIS}}) \quad \forall t \in \mathcal{T}, c, r \in \mathcal{C} \quad (1f)$$

$$z_{c,d} \leq \Lambda_{c,d}^{\text{BH}} (y_c^{\text{IAB}} \wedge y_d^{\text{IAB}}) \quad \forall c, d \in \mathcal{C} \quad (1g)$$

$$\sum_{c,r \in \mathcal{C}} x_{t,c,r} = 1 \quad \forall t \in \mathcal{T} \quad (1h)$$

$$w_c + \sum_{d \in \mathcal{C}} (f_{d,c} - f_{c,d}) - \sum_{t \in \mathcal{T}} \sum_{r \in \mathcal{C}} D x_{t,c,r} = 0 \quad \forall c \in \mathcal{C} \quad (1i)$$

$$w_c \leq U^{WRD} y_c^{\text{DON}} \quad \forall c \in \mathcal{C} \quad (1j)$$

$$f_{c,d} \leq z_{c,d} U_{c,d} \quad \forall c, d \in \mathcal{C} \quad (1k)$$

$$D x_{t,c,r} \leq V_{t,c,r}^{\text{DIR}} \quad \forall t \in \mathcal{T}, c, r \in \mathcal{C} \quad (1l)$$

$$\xi D x_{t,c,r} \leq V_{t,c,r}^{\text{REF}} \quad \forall t \in \mathcal{T}, c, r \in \mathcal{C} \quad (1m)$$

$$t_c^{\text{TX}} = \sum_{d \in \mathcal{C}} \frac{f_{c,d}}{U_{c,d}} + \sum_{t \in \mathcal{T}, r \in \mathcal{C}} \frac{D_t x_{t,c,r}}{V_{t,c,r}^{\text{DIR}}} \quad \forall c \in \mathcal{C} \quad (1n)$$

$$t_c^{\text{RX}} = \sum_{d \in \mathcal{C}} \frac{f_{d,c}}{U_{d,c}} \quad \forall c \in \mathcal{C} \quad (1o)$$

$$t_c^{\text{TX}} + t_c^{\text{RX}} \leq y_c^{\text{IAB}} \quad \forall c \in \mathcal{C} \quad (1p)$$

$$\sum_{d \in \mathcal{C}} z_{c,d} \leq 1 - y_c^{\text{DON}} \quad \forall c \in \mathcal{C} \quad (1q)$$

$$\tau_{t,c,r} \leq x_{t,c,r} \quad \forall t \in \mathcal{T}, c, r \in \mathcal{C} \quad (1r)$$

$$\sum_{t \in \mathcal{T}, c \in \mathcal{C}} \tau_{t,c,r} \leq y_r^{\text{RIS}} \quad \forall r \in \mathcal{C} \quad (1s)$$

<sup>2</sup>While a vertical field of view usually has a limited impact on the final network plan, it can be easily included in the model, if needed.

<sup>3</sup>As it will be explained later, the donor installation cost is considered as a fixed expense. Thus it is not modelled into a parameter.

$$\sum_{c,r \in \mathcal{C}} \tau_{t,c,r} V_{t,c,r}^{DIR} \geq D \quad \forall t \in \mathcal{T} \quad (1t)$$

$$\phi_r \geq \Phi_{r,t}^A - F/2 - 2\pi(\neg x_{t,d,r}) \quad \forall t \in \mathcal{T}, d, r \in \mathcal{C} \quad (1u)$$

$$\phi_r \leq \Phi_{r,t}^A + F/2 + 2\pi(1 - x_{t,d,r}) \quad \forall t \in \mathcal{T}, d, r \in \mathcal{C} \quad (1v)$$

$$\phi_r \geq \Phi_{r,d}^B - F/2 - 2\pi(1 - x_{t,d,r}) \quad \forall t \in \mathcal{T}, d, r \in \mathcal{C} \quad (1w)$$

$$\phi_r \leq \Phi_{r,d}^B + F/2 + 2\pi(1 - x_{t,d,r}) \quad \forall t \in \mathcal{T}, d, r \in \mathcal{C} \quad (1x)$$

$$\theta_t \leq \Theta_{t,c,r} + 2\pi(1 - x_{t,c,r}) \quad \forall t \in \mathcal{T}, c, r \in \mathcal{C} \quad (1y)$$

$$\lambda_t \geq \frac{1}{2} \sum_{c,r \in \mathcal{C}} x_{t,c,r} (L_{t,r} + L_{t,d}) \quad \forall t \in \mathcal{T} \quad (1z)$$

The objective function (1a) maximizes the average angular separation over the planned network while minimizing the average link length. In particular, parameters  $\Theta$  and  $\bar{L}$  are used to normalize the angular separation sum and link length sum over all TPs, while parameter  $\mu \in [0, 1]$  can be used to tune the maximization emphasis toward one of the two objectives.

Constraint (1b) makes sure that IAB nodes and RISes are not installed in the same CS.

From a modelling standpoint, a donor is equivalent to an IAB node connected to the core network. Consequently, a donor can only be active in a candidate site populated by an IAB node, as stated by constraint (1c). Constraint (1d) allows for the activation of exactly one donor<sup>4</sup>, which becomes a fixed planning expense not considered in budget constraint (1e).

Using binary link activation parameters  $\Lambda_{t,c,r}^{\text{SRC}}$ , constraint (1f) allow for an SRC variable to be active only if the necessary radio connections can be established and if the BS and RIS involved in the SRC are installed. Similarly, constraint (1g) allows for a backhaul link to be active only if the two nodes are installed, and a radio connection can be established between the two. For the sake of compactness, we have expressed the two constraints above through logical *and* operator  $\wedge$ , which are easily linearized at solving time. Constraint (1h) makes sure that each TP is covered by one SRC.

For each node, the traffic flow entering from the core network and the parent IAB node is balanced with the traffic leaving the node towards the associated UEs and downstream IAB nodes through constraint (1i). Note that the traffic coming from the core is available only at the donor, and it is limited by a wired capacity parameter  $U^{\text{WRD}}$ , as stated in constraint (1j). Similarly, the traffic flowing through each active backhaul link is limited by the link's capacity in constraint (1k).

Constraints (1l) and (1m) are such that an SRC can be activated only if it can support both the direct and reflected link demands.

Constraints (1n), (1o) and (1p) enforce half-duplexing for each BS, by considering the time spent transmitting to downstream IAB nodes, to associated UEs and the time spent receiving data from upstream IAB nodes.

According to standard specifications, IAB networks are ex-

pected to assume spanning-tree topology [22]. In our model, constraint (1q) enforces the creation of a spanning tree by allowing for up to one ingress link per IAB node and none for the donor.

While each RIS can be part of multiple SRCs, we allow only one TX-RX pair to be served at any time by a single RIS. Each reconfigurable surface is thus shared among different SRCs through a time-division process, as previously mentioned. Variables  $\tau_{t,c,r}$ , representing the fraction of time spent by RIS  $r$  while assisting the communication between BS  $c$  and TP  $t$ , can be larger than zero only if the corresponding SRC is active and the RIS is installed, as stated in constraints (1r) and (1s). Since the direct link can encounter blockages at any time, we force the RIS to be available for the entire transmission duration, such that the reflected link can always be employed. Constraint (1t) captures this behaviour, reserving RIS time-sharing capacity for each SRC that makes use of it.

Constraints from (1u) to (1x) set each RIS's orientation such that the associated BSs and UEs all fall inside its field of view  $F$ , which is achieved by considering parameters  $\Phi_{r,t}^A$  and  $\Phi_{r,d}^B$ . These represent the angles between the line connecting the RIS  $r$  to TP  $t$  or to CS  $c$ , respectively, and the reference direction.

Finally, constraint (1y) sets  $\theta_t$  to the minimum angular separation between the line connecting the TP with the associated BS and the line connecting the TP with the associated RIS. Constraint (1z) sets  $\lambda_t$  to the average between the BS-TP link length and the RIS-TP link length.

#### IV. RESULTS

In this section, we give a numerical analysis of the previously described model when applied to random planning instances. Furthermore, we compare the results given by RIS-enabled planning against a baseline approach where only donors and IAB nodes can be installed. In this case, dual connectivity is still guaranteed by covering each TP with two different base stations instead of relying on a RIS-reflected path. However, apart from the alternative radio link nature, all the planning assumptions and objectives remain unchanged, as well as the parameters that follow.

The considered planning instances are characterized by a deployment area of  $300 \times 400m$  where 25 CSs can be activated, and 15 TPs need to be covered.

Donors and IAB nodes are modelled as 64-elements uniform linear array antennas with transmission power of  $30dBm$  and carrier frequency set to  $28GHz$ . Receivers are modelled as omnidirectional antennas. RISes are modeled as planar surfaces of  $50 \times 50cm$  containing  $10^4$  passive reflecting elements, which is compatible with a  $\lambda/2$  inter-element spacing [23]. The path-loss model of [21] and the received power formulas in [6] were employed to precompute the average SNR of the links of every SRC combination. Finally, achievable rates were extracted according to NR modulation and coding scheme [24].

Primary TP traffic demand is set to  $100Mbps$ . The degradation factor  $\xi$  is set to 0.5, leading to a secondary

<sup>4</sup>Given that IAB nodes and UEs can receive downlink traffic only from one donor, multiple donors would span independent IAB network that could be separately planned

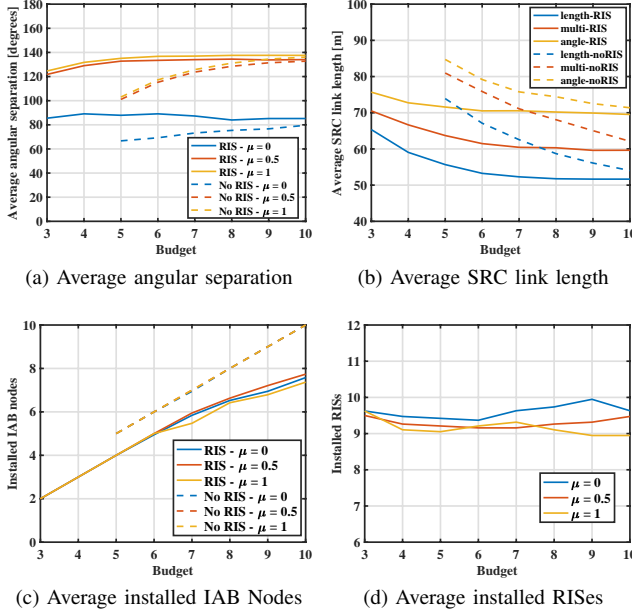


Fig. 2: Budget variations, from 3 to 10 units with 1 unit increments.

demand of  $50\text{Mbps}$  guaranteed on each secondary link. All the results in this section were obtained by averaging 20 random drops of CS and TP positions. Random instances were generated though MATLAB and planning optimization was solved by CPLEX.

#### A. Budget Sensitivity

We present the budget sensitivity analysis by evaluating the blockage resilience indicators, i.e. average angular separation and link length, for different budget planning values. A clear indication of the cost of deploying an RIS has yet to be found in the literature. However, prototypes have shown how RISes can be realized with inexpensive materials and production processes. Thus, an order of magnitude between the cost of IAB nodes and RISes seems reasonable. Consequently, we have set to 1 the cost of deploying an IAB node<sup>5</sup> and to 0.1 the price of installing an RIS.

In Figures 2a and 2c we plot the blockage resilience indicators against a planning budget that spans from 3 to 10 units. In particular, in Figure 2a we compare the average angular separation of RIS-enabled planning (solid lines) and IAB-only planning (dashed lines). The comparison is carried out by considering different values of  $\mu$  in the objective function (1a). Namely, we evaluated the results when either only the maximization of the average angular separation is considered ( $\mu = 1$ ), or when only the minimization of the link length is considered ( $\mu = 0$ ). Furthermore, we have analyzed  $\mu = 0.5$ , which represents a balance between the two objectives. A similar analysis is shown in Fig. 2b for the average SRC link length.

In both figures and for any considered  $\mu$ , the dotted lines corresponding to the baseline approach are interrupted for

<sup>5</sup>Note that, since a donor BS is always installed, its installation price is considered as a fixed expenditure.

$B < 5$ . No solution could be found with these budget values (i.e., minimum rate cannot be guaranteed). On the other hand, RIS-enabled planning is still feasible for these values, showing how RISes can be used to solve planning scenarios with strict budgets.

As the budget increases past 5 units, the baseline approach can be brought to a solution. However, RIS-enabled planning generally outperforms the IAB-only approach in terms of both angular separation and link length. Indeed, a budget increase of approximately 40% is required such that the IAB-only model can reach the same level of angular separation and link length of RIS-enabled planning.

This behaviour is due to the reduced RIS installation costs that allow a larger number of RISes to be installed even with lower budgets. In particular, Figures (2c) and (2d) show how the number of installed RISes is always considerably larger than the installed IAB nodes, especially for low  $B$  values. Moreover, one can notice in Figure (2c) how the average installed IAB nodes for the baseline approach (dashed lines) is always 1 to 3 nodes higher than the case when RISes can be installed (solid lines). This suggests that, while the number of necessary IAB nodes can be reduced by employing RISes, these cannot be considered a full substitute of IAB nodes since a relatively high number of them need to be active. On the other hand, Figure (2d) shows how RIS installation is not heavily affected by budget availability, which is expected considering the cost installation ratio.

#### B. Obstacle Deployment

As it is stated in Sec. III, the objective of our proposed planning solution is to optimize some topological properties to strengthen the planned radio access network against blockages due to line of sight obstructions. We now evaluate the resilience of the resulting planned networks during normal operation conditions. To do this, we drop randomly oriented, 5 meters long obstacles into random positions of the planning area. Additionally, we have added a self-blockage angular sector, representing the human body obstruction, to each TP. The angle span is either  $2\pi/3$  or  $8\pi/9$  with a probability of 0.5 each, and it is randomly oriented [25]. Any radio link that falls inside the self blockage sector or that is crossed by a randomly dropped obstacle is considered blocked.

Figure 3a shows the percentage of served TPs (i.e., at least one between primary and secondary link is not blocked) for an increasing number of dropped obstacles and a planning budget of 5 units. In general, the baseline approach (dashed lines) is consistently outperformed by the RIS-enabled (solid lines), confirming the results of the previous paragraph. Indeed, Figure 3b shows that RIS-enabled planning results in up to 50% more served TPs with respect to the baseline approach. Additionally, Figure 3a shows how the link length-minimizing objective function ( $\mu = 0$ ) outperforms the other two objective approaches as soon as the dropped obstacles increase past 300. This suggests that the planning objective should be chosen according to the expected obstacle density.

As previously mentioned, higher budget levels allow for the



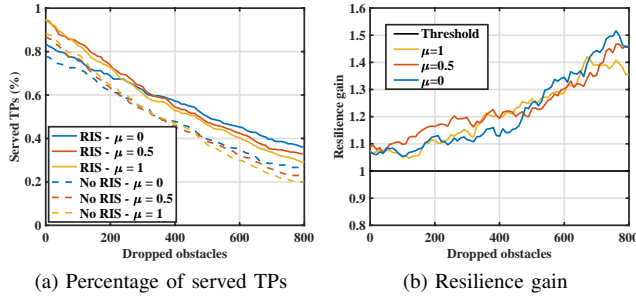


Fig. 3: Impact of obstacles on TPs in outage,  $B = 5$ .

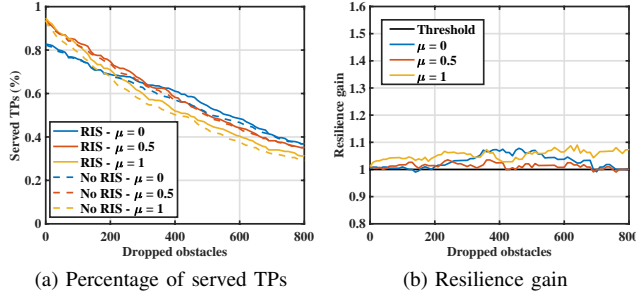


Fig. 4: Impact of obstacles on TPs in outage,  $B = 10$ .

installation of more IAB nodes, and the objective function values of the baseline converge to those of the RIS-enabled planning. Consequently, the resilience gain of the RIS-based approach is shortened for  $B = 10$ , as shown in Figure 4.

In particular, Figure 4a shows a reduced difference between the percentage of served TPs of the baseline and RIS-enabled approach when the budget value is set to 10 units. Similarly, the resilience gain of using RISes with  $B = 10$ , in Figure 4b, is limited to a maximum of 10%.

Finally, these results confirm that RISes are better employed in budget-restricted planning scenarios, as they effectively provide cost-effective blockage resilience through densification.

## V. CONCLUSION

We described the problem of planning a mm-Wave IAB RAN with RISes aiming at the maximization of resilience against obstructions and self-blockages. In particular, we proposed a MILP network planning model that privileges topological characteristics such as angular separation and link length, proven to be effective in enhancing RAN reliability. In our simulation campaigns, we have compared the results of the RIS-enabled planning against a baseline approach where no RIS is installed. Numerical results showed an increase in access resilience and a reduction in budget expenditure through the usage of RISes, compared to a more traditional model.

## ACKNOWLEDGMENT

The research in this paper has been carried out in the framework of Huawei-Politecnico di Milano Joint Research Lab. The Authors acknowledge Huawei Milan research center for the collaboration.

## REFERENCES

- [1] T. S. Rappaport, Y. Xing, O. Kanhere *et al.*, "Wireless communications and applications above 100 ghz: Opportunities and challenges for 6g and beyond," *IEEE Access*, vol. 7, pp. 78 729–78 757, 2019.
- [2] F. Devoti and I. Filippini, "Planning mm-wave access networks under obstacle blockages: A reliability-aware approach," *IEEE/ACM Trans. on Networking*, vol. 28, no. 5, pp. 2203–2214, 2020.
- [3] M. Polese, M. Giordani, T. Zugno *et al.*, "Integrated access and backhaul in 5g mmwave networks: Potential and challenges," *IEEE Comm. Mag.*, vol. 58, no. 3, pp. 62–68, 2020.
- [4] E. Basar, M. Di Renzo, J. De Rosny, M. Debbah, M. Alouini, and R. Zhang, "Wireless communications through reconfigurable intelligent surfaces," *IEEE Access*, vol. 7, pp. 116 753–116 773, 2019.
- [5] M. Di Renzo, K. Ntontin, J. Song *et al.*, "Reconfigurable Intelligent Surfaces vs. Relaying: Differences, Similarities, and Performance Comparison," *IEEE Open Jrm. of the Comm. Society*, pp. 1–1, jun 2020.
- [6] P. Wang, J. Fang, X. Yuan, Z. Chen, and H. Li, "Intelligent reflecting surface-assisted millimeter wave communications: Joint active and passive precoding design," *IEEE Trans. on Vehic. Tech.*, vol. 69, no. 12, pp. 14 960–14 973, 2020.
- [7] E. Amaldi, A. Capone, M. Cesana, I. Filippini, and F. Malucelli, "Optimization models and methods for planning wireless mesh networks," *Comp. Networks*, vol. 52, no. 11, pp. 2159–2171, 2008.
- [8] A. Capone, M. Cesana, D. De Donno, and I. Filippini, "Deploying multiple interconnected gateways in heterogeneous wireless sensor networks: An optimization approach," *Comp. Comm.*, vol. 33, no. 10, pp. 1151–1161, 2010.
- [9] J. Y. Lai, W.-H. Wu, and Y. T. Su, "Resource allocation and node placement in multi-hop heterogeneous integrated-access-and-backhaul networks," *IEEE Access*, vol. 8, pp. 122 937–122 958, 2020.
- [10] B. Marques, M. Sousa, P. Vieira, M. Queluz, and A. Rodrigues, "Automated joint access and backhaul planning for 5g millimeter-wave small cell networks," in *IEEE WPMC*, 2020, pp. 1–6.
- [11] C. Madapatha, B. Makki, A. Muhammad, E. Dahlman, M.-S. Alouini, and T. Svensson, "On topology optimization and routing in integrated access and backhaul networks: A genetic algorithm-based approach," *arXiv:2102.07252*, 2021.
- [12] H. Gacanin and M. Di Renzo, "Wireless 2.0: Toward an intelligent radio environment empowered by reconfigurable meta-surfaces and artificial intelligence," *IEEE Vehic. Tech. Mag.*, vol. 15, no. 4, pp. 74–82, 2020.
- [13] Q. Wu and R. Zhang, "Towards smart and reconfigurable environment: Intelligent reflecting surface aided wireless network," *IEEE Comm. Mag.*, vol. 58, no. 1, pp. 106–112, 2019.
- [14] C. Huang, A. Zappone, G. C. Alexandropoulos, M. Debbah, and C. Yuen, "Reconfigurable intelligent surfaces for energy efficiency in wireless communication," *IEEE Trans. on Wirel. Comm.*, vol. 18, no. 8, pp. 4157–4170, 2019.
- [15] M. Di Renzo, K. Ntontin, J. Song, F. H. Danufane, X. Qian, F. Lazarakis, J. De Rosny, D.-T. Phan-Huy, O. Simeone, R. Zhang *et al.*, "Reconfigurable intelligent surfaces vs. relaying: Differences, similarities, and performance comparison," *IEEE Open Jrm. of the Comm. Society*, vol. 1, pp. 798–807, 2020.
- [16] E. Björnson, Ö. Özdogan *et al.*, "Intelligent reflecting surface versus decode-and-forward: How large surfaces are needed to beat relaying?" *IEEE Wirel. Comm. Lett.*, vol. 9, no. 2, pp. 244–248, 2019.
- [17] M. A. Kishk and M.-S. Alouini, "Exploiting randomly-located blockages for large-scale deployment of intelligent surfaces," *IEEE Jrm. on Sel. Areas in Comm.*, 2020.
- [18] E. Moro, I. Filippini, A. Capone, and D. D. Donno, "Planning mm-wave access networks with reconfigurable intelligent surfaces," *arXiv:2105.11755*, 2021.
- [19] M. Di Renzo, M. Debbah, D.-T. Phan-Huy *et al.*, "Smart radio environments empowered by reconfigurable ai meta-surfaces: An idea whose time has come," *EURASIP Jrm. on Wirel. Comm. and Networking*, vol. 2019, no. 1, pp. 1–20, 2019.
- [20] T. Bai and R. W. Heath, "Analysis of self-body blocking effects in millimeter wave cellular networks," in *2014 48th Asilomar Conf. on Signals, Systems and Comp.*, 2014, pp. 1921–1925.
- [21] M. R. Akdeniz, Y. Liu, M. K. Samimi, S. Sun, S. Rangan, T. S. Rappaport, and E. Erkip, "Millimeter wave channel modeling and cellular capacity evaluation," *IEEE Jrm. on Sel. Areas in Comm.*, vol. 32, no. 6, pp. 1164–1179, 2014.
- [22] 3GPP, "NR; Study on integrated access and backhaul," Technical Specification (TS) 38.3874, 01 2019, version 16.0.0.

- [23] M. D. Renzo, A. Zappone, M. Debbah *et al.*, “Smart Radio Environments Empowered by Reconfigurable Intelligent Surfaces: How it Works, State of Research, and Road Ahead,” *IEEE Jrn. on Sel. Areas in Comm.*, 2020.
- [24] 3GPP, “NR; Physical layer procedures for data,” Technical Specification (TS) 38.204, 03 2021, version 16.5.0.
- [25] 3GPP RAN Group, “Study on Channel Model for Frequencies From 0.5 to 100 GHz (Release 15),” *Document TR 38.901*, 2020.